Available online at www.sciencedirect.com
ScienceDirect
Advances in Space Research 47 (2011) 2140–2151
ADVANCES IN SPACE RESEARCH (a COSPAR publication)
www.elsevier.com/locate/asr

Why should the latitude of the observer be considered when modeling gradual proton events? An insight using the concept of cobpoint

R. Rodríguez-Gasén [a,*], A. Aran [b], B. Sanahuja [a], C. Jacobs [c], S. Poedts [c]

[a] Departament d'Astronomia i Meteorologia and Institut de Ciències del Cosmos, Universitat de Barcelona, Martí i Franquès 1, E-08028 Barcelona, Spain
[b] Research and Scientific Support Department of European Space Agency, ESTEC, Keplerlaan 1, 2200 AG Noordwijk, The Netherlands
[c] Centrum Voor Plasma Astrofysica, Katholieke Universiteit Leuven, Celestijnenlaan 200B, B-3001 Leuven, Belgium

Received 1 August 2009; received in revised form 18 February 2010; accepted 11 March 2010
Available online 18 March 2010

Abstract

The shape of flux profiles of gradual solar energetic particle (SEP) events depends on several not well-understood factors, such as the strength of the associated shock, the relative position of the observer in space with respect to the traveling shock, the existence of a background seed particle population, the interplanetary conditions for particle transport, as well as the particle energy. Here, we focus on two of these factors: the influence of the shock strength and the relative position of the observer. We performed a 3D simulation of the propagation of a coronal/interplanetary CME-driven shock in the framework of ideal MHD modeling. We analyze the passage of this shock by nine spacecraft located at ~0.4 AU (Mercury's orbit) and at different longitudes and latitudes. We study the evolution of the plasma conditions in the shock front region magnetically connected to each spacecraft, that is the region of the shock front scanned by the "cobpoint" (Heras et al., 1995), as the shock propagates away from the Sun. Particularly, we discuss the influence of the latitude of the observer on the injection rate of shock-accelerated particles and, hence, on the resulting proton flux profiles to be detected by each spacecraft.

Keywords: Space weather; Solar energetic particle events; Shocks; MHD simulations; Coronal mass ejections

1. Introduction

After an initial suggestion by Evenson et al. (1982), in late 1980s it became clear that the interplanetary component of gradual solar energetic particle (SEP) events is more important than the solar component itself. This implies that the large-scale topology of interplanetary shocks plays a key role in the development of gradual SEP events and that their time-intensity profiles display an organization with respect to the heliolongitude of the solar parent event (e.g., Cane et al., 1988; Domingo et al., 1989; Reames, 1990; Richardson et al., 1991). The observed intensity profiles are understood as a superposition of particles continuously accelerated at the sun-outward propagating shock, with their properties modified later on by their subsequent propagation along the interplanetary magnetic field (IMF). In this sense, we talk about the efficiency of the shock as injector of accelerated particles (Heras et al., 1992). Heras et al. (1992, 1995) simulated several SEP events showing how this shock efficiency evolves, both because the shock propagates and expands and because the magnetic connection of the observer to the front of the shock moves eastward along its front. Therefore, different intensity profiles result from different relative locations of the observer with respect to the nose of the shock. So, these profiles depend on the magnetic connection between the observer and the front of the shock.

The concept of observer-shock front magnetic connection was first explicitly considered in modeling by Heras et al. (1995). It was named "cobpoint" (Connecting with

* Corresponding author. Tel.: +34 606249264; fax: +34 934021133.
E-mail address: rrodriguez@am.ub.es (R. Rodríguez-Gasén).

0273-1177/$36.00 © 2010 COSPAR. Published by Elsevier Ltd. All rights reserved.
doi:10.1016/j.asr.2010.03.021

the OBserver POINT) by analogy with "footpoint" (the solar root of an IMF line), but with the difference that the cobpoint is associated with an interplanetary mobile source of particles. Thus, at a given time, for a given position of the interplanetary shock, observers in space located at different radial distances or heliolongitudes will define different cobpoints in the shock front (see, for example, Lario et al., 1998; Aran et al., 2007).

In addition to the heliolongitude and the particles energy range, there are other factors that play a role in determining the shape of the time-intensity profiles of SEP events: the strength of the shock, its evolution (size, velocity and shape) and the presence of a seed particle population to be further accelerated, as well as the conditions of the particle transport in interplanetary space (e.g., Cane et al., 1988; Lario et al., 1998; Kahler, 2001). Cane and Lario (2006) provided a list of elements that future SEP models should include; among them, 3D MHD simulations of the shock, starting close to the Sun (i.e., at few solar radii).

This paper presents an insight in part of these items, mainly addressing the potential relevance of the heliocentric latitude (i.e., latitudinal angular location of the observer with respect to the interplanetary shock) and the evolution of the shock strength at the cobpoint. A first attempt discussing the variations of the conditions of the particle acceleration at traveling shocks was presented by Manchester et al. (2005). Nevertheless, the influence of the latitude has not been quantitatively considered in simulations of gradual SEP events yet, essentially because most of the MHD codes used until now to model shocks associated with gradual SEP events are 1D, 2D or 2.5D MHD codes (e.g., Li et al., 2005; Aran et al., 2007; Verkhoglyadova et al., 2009). The scarce number of attempts to simulate SEP events using 3D MHD models for CME propagation have been applied to near-ecliptic SEP observations (e.g., Sokolov et al., 2004; Luhmann et al., 2007). The evolution near the Sun of the shock variables at the cobpoint is important to reproduce the prompt phase of many gradual events, specially for west and central meridian events and at high energies.

Specifically, we simulate a 3D CME-driven shock and we follow its evolution up to 100 $R_\odot$. We analyze some plasma variables and quantify their jumps (downstream-to-upstream ratios) across the shock front at the cobpoint position of nine virtual spacecraft situated at 86 $R_\odot$, at three different longitudes and latitudes. Our aim is to study the influence of the strength of the shock on the injection rate of shock-accelerated particles and, thus, on the resulting SEP flux profiles. Section 2 describes the MHD model used to simulate the shock, the background solar wind adopted and the initial conditions assumed for the CME perturbation. Section 3 shows the procedure used in the analysis of the plasma variables at the cobpoint position. Section 4 presents the results and the discussion, and in Section 5 we give the conclusions.

2. The 3D MHD shock simulation

We use the Versatile Advection Code (Tóth, 1996), a finite volume shock capturing code working on structured grids, to perform a 3D MHD simulation of the CME-driven shock. The ideal MHD equations are solved in spherical coordinates and the computational domain extends from 1 to 220 $R_\odot$ in the radial direction from the Sun, r, from $-90°$ to $90°$ in latitude, θ, and from $0°$ to $360°$ in longitude, φ. The grid resolution is of $1104 \times 95 \times 184$ points including four ghost-cells for each direction and it has an accumulation of cells towards the Sun and towards the equator. The radial step varies from $\delta r = 0.02$ $R_\odot$ near 1 $R_\odot$ to $\delta r = 0.24$ $R_\odot$ from 30 $R_\odot$ on; this high resolution is necessary to get a good capture of the shock structure. The grid in the θ-direction also varies from a maximum angular step near the poles, $\delta\theta = 3.88°$, to a minimum value at the equator, $\delta\theta = 0.8°$. In the ϕ-direction the grid is uniform, with $\delta\phi = 2°$. Divergence-free magnetic field is guaranteed at all time by using the vector potential at the nodes according to the constrained transport method (Evans and Hawley, 1988).

The initial condition for the axisymmetric background solar wind is the hydrodynamic solution of Parker (1958), with a supplementary dipolar magnetic field of 2.10×10^5 nT at the poles. As the initial solution relaxes to reach the steady state, the original magnetic dipole configuration is lost and regions of open and closed field lines develop. The ratio of the specific heats is set to $\gamma = 5/3$ and the initial conditions at the solar base (1 $R_\odot$) are: $\rho_0 = 1.67 \times 10^{-16}$ g cm^{-3}, $T_0 = 1.50 \times 10^6$ K, and $\Omega_0 = 2.77 \times 10^{-6}$ rad s^{-1} for the solar angular velocity. In order to reproduce a fast and a slow solar wind regime, an additional heating term in the energy equation has to be considered (Groth et al., 2000). We adopt for this term the expressions given by Manchester et al. (2004a,b), frequently used in simulations (Lugaz et al., 2005a,b; Jacobs et al., 2007).

Fig. 1 presents several solar wind profiles as a function of the radial distance (left) and of the latitude (right). From top to bottom the three panels display the magnetic field, B, number density, n, and radial velocity, v_r, profiles. Each panel shows three curves, corresponding to latitudes: $\theta = 22°$, the latitude of the CME-launch direction (see below), $\theta = 7°$, approximately the maximum latitude of the ecliptic plane and $\theta = 45°$. In the bottom panel, two regimes of solar wind can be clearly differentiated: a fast regime ($\sim$600–800 km s^{-1}) at high latitudes and a slow regime ($\sim$400 km s^{-1}) near the equator. The three right panels show the dependence of the same variables with latitude at 15 $R_\odot$.

To simulate the CME-driven shock, we use a density-driven pulse to trigger the CME (Jacobs, 2007). The shock is generated by superimposing a high-density plasma blob on the background solar wind, with a certain velocity v_{cme} in a given direction $(\theta_{cme}, \varphi_{cme})$. The velocity and density profiles of the initial disturbance are given by

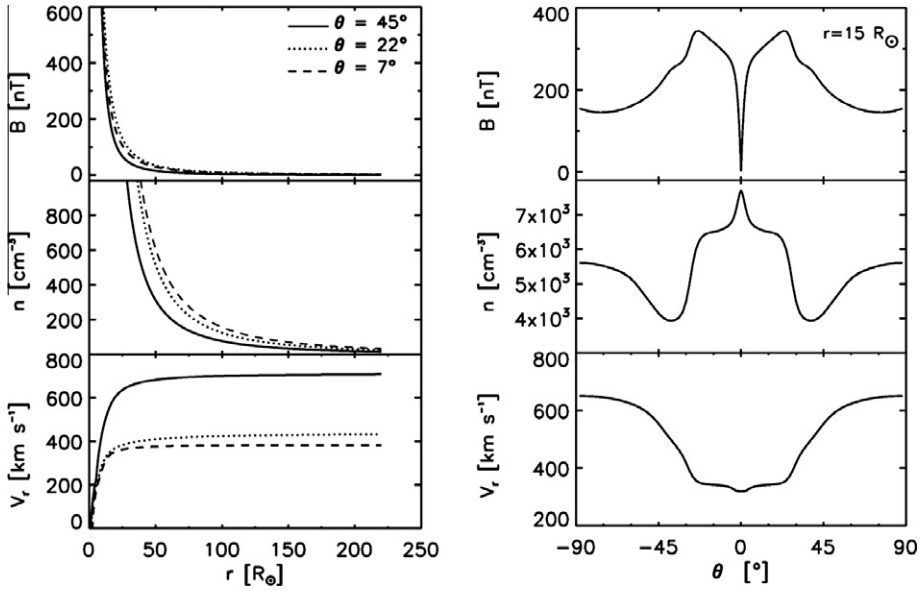

Fig. 1. Left panels: B, n and υ_r profiles for the background solar wind as a function of the radial position for three latitudes: 45° (solid line); 22° (dotted line); 7° (dashed line). Right panels: The same profiles as in the left panels but displayed as a function of the latitude at $r = 15\ R_\odot$.

$$X = \frac{X_{cme}}{2}\left(1 - \cos\pi\frac{d_{cme} - d}{d_{cme}}\right), \tag{1}$$

where X indicates density or radial velocity, and X_{cme} its maximum value inside the blob; d is the distance to the center of the blob and d_{cme} is its radius (see Jacobs et al. (2005; Jacobs, 2007), for more details).

The center of the initial plasma blob is situated at 2.5 $R_\odot$ and it is launched in direction ($\theta_{cme} = 22°, \varphi_{cme} = 142°$). We assume $d_{cme} = 0.75\ R_\odot, \rho_{cme} = 7 \times 10^8\ cm^{-3}$ and $\upsilon_{cme} = 3500\ km\ s^{-1}$. These values yield a total mass of $\sim 1.4 \times 10^{17}$ g and a kinetic energy of $\sim 2.5 \times 10^{33}$ erg; both quantities are within the range of estimated values for fast CMEs (Vourlidas et al., 2002; Manchester et al., 2006, 2008; Colaninno and Vourlidas, 2009). As a guide, one run from the Sun up to $\sim 100\ R_\odot$ takes about 48,000 h of elapsed time using 440 processors of the VIC cluster at the Katholieke Universiteit Leuven.

3. The cobpoint and shock-normal calculation procedure

The evolution of the simulated shock is followed up to 100 $R_\odot$, as seen by nine observers located at 86 $R_\odot$ from the Sun ($\sim$0.4 AU) and placed at three different longitudes and latitudes. We use the Heliocentric Earth Equatorial (HEE) system of reference (Hapgood, 1992) to identify the position of the observer. The X-axis is the intersection between the solar equator and the central meridian as seen from the Earth, the Z-axis is the rotation axis of the Sun. The Y-axis is perpendicular to both on them in the equatorial plane, completing the right-handed system. For example, in this reference system an observer placed in the direction of the launch of the CME (i.e., the same direction as the nose of the shock driven by the CME) has the coordinates: N22W00.

In longitude, we place three observers 45° westward and 30° eastward from the nose of the shock, and other three in the same longitude as the CME-launch direction; thus, at W45, E30 and W00 longitude, respectively. In latitude, three observers are placed at the same latitude as the CME leading direction, $\theta = 22°$, they are the N22 observers. Other three observers are placed 15° northward of this direction and three more 15° southward. So, they are N37 and N07 observers, respectively.

In short, the nine observers are located at N37W45, N22W45, N07W45, N37W00, N22W00, N07W00, N37E30, N22E30 and N07E30, with the CME launched in the N22W00 direction. In this way we can evaluate the values of the plasma and magnetic field variables upstream, at the passage and downstream of the shock front, as well as their changes due to the vantage position of the observers. Fig. 2 shows these observers as colored solid circles under three different 3D perspectives.

The spiral IMF line passing through each observer is constructed from the MHD simulation. Starting from the observer's position, we search for the cobpoint location along the IMF line by requiring a radial velocity threshold of 1% over the background solar wind, that is $\xi = (\upsilon_r - \upsilon_{r_{sw}})/\upsilon_{r_{sw}} > 0.01$. We considered different values for this threshold (from 0.01% to 0.5%), concluding that the adopted value is a good choice because, for the set of studied observers, the differences in distance found in the identification of the cobpoint position are small (in average, smaller than 0.04 $R_\odot$ and only for one case $\sim$0.5 $R_\odot$).

Fig. 2 shows three different views of one snapshot of the shock simulation 4.95 h after the CME launch, as well as the situation of the nine observers. Top left and top right

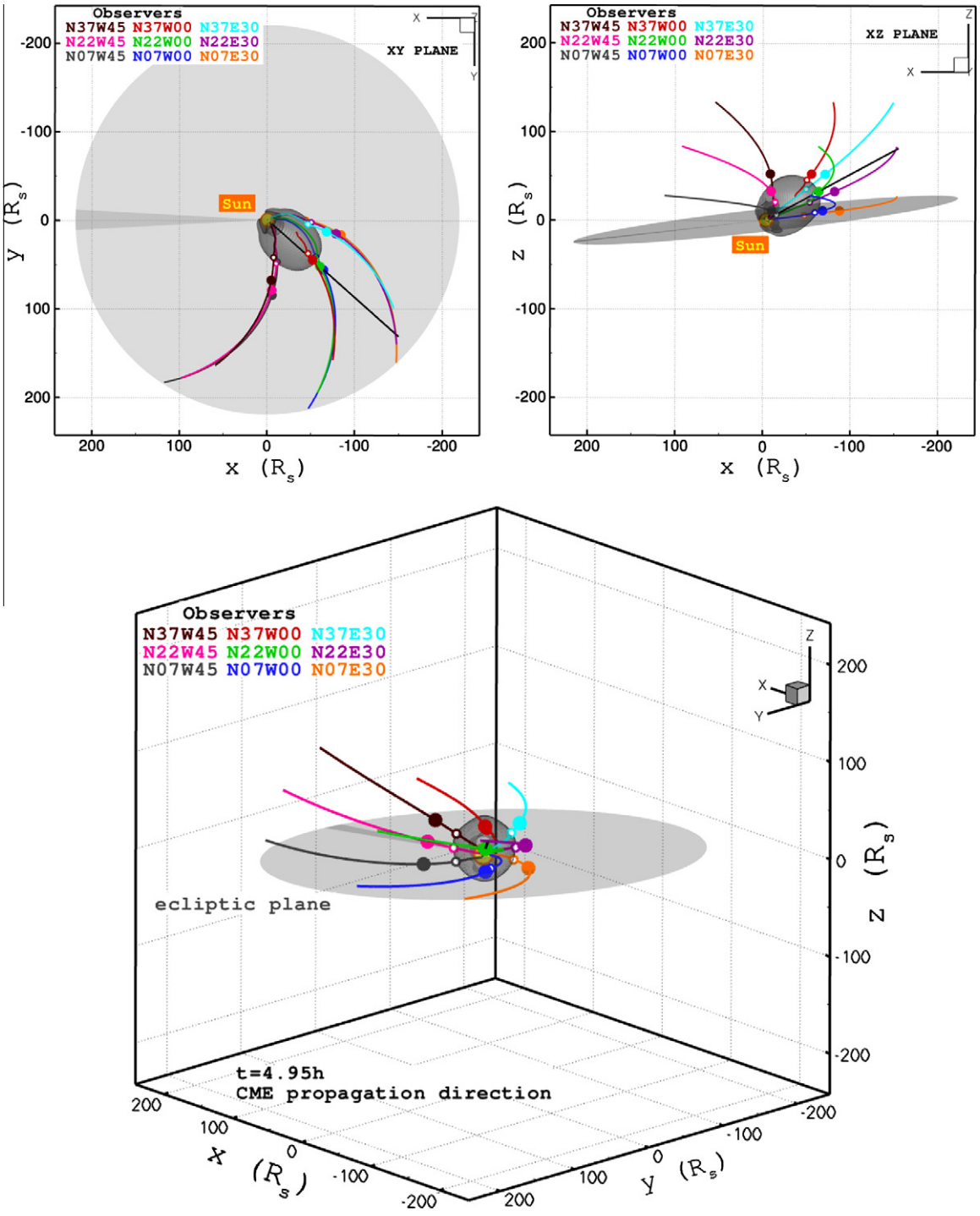

Fig. 2. Three views of a snapshot of the 3D simulation after $t = 4.95$ h. Top left: the XY plane; top right: the XZ plane; bottom: 3D frontal view. The dark-grey isosurface indicates $\xi = 0.01$ (see the text). The gray slice shows the ecliptic plane, the Sun is located by the yellow point and the black line indicates the CME propagation direction. The color code for the nine observers, their corresponding IMF lines and cobpoints are given in the text.

panels show a view of the XY and XZ plane, respectively; bottom panel displays a 3D frontal view of the simulation. The dark-gray surface indicates the regions of the CME where the relative radial velocity coincides with the threshold value. This surface marks the spatial boundary of the front of the expanding interplanetary shock. The black line indicates the CME propagation direction. The yellow point shows the location of the Sun and the gray disc the ecliptic plane. Colored solid circles indicate the position of the nine observers, the color lines their IMF lines and the colored open circles the location of their corresponding cobpoints. The color code for the nine observers is as follows:

N37W45, brown; N22W45, pink; N07W45, dark-gray; N37W00, red; N22W00, green; N07W00, blue; N37E30, cyan; N22E30, purple; N07E30, orange.

Once the cobpoint has been identified, it is necessary to determine the direction of the shock normal, $\hat{n}$, at this point, in order to further calculate the plasma jumps across the shock front. To compute $\hat{n}$ we can figure out that the simulated shock reproduces a real interplanetary shock, with the observer located at the cobpoint when the shock front sweeps its position. Hence, it is necessary to find a "downstream point" (in real cases the downstream region is chosen after visual inspection), where the values of the plasma variables and magnetic field have to be picked up. As first estimate, we search for it along the radial direction from the cobpoint, moving on toward the Sun; the first point where the derivative of the relative radial velocity is smaller than 20% of the maximum value of this derivative along the radial line, is chosen as first approach- or tempative-downstream point.

Near the nose of the shock the plasma jumps derived directly from observations might probably be quite similar to those derived in the normal direction, but this may not be true when the cobpoint is too distant from the central part of the shock (either in longitude or latitude). Then, we can use any of the various and well documented existing methods to determine the shock-normal direction (e.g., Viñas and Scudder, 1986; Szabo, 1994; Berdichevsky et al., 2000; Lin et al., 2006; Koval and Szabo, 2008 and references quoted there). We have selected five of them: (i) the magnetic field coplanarity method, MC (Colburn and Sonett, 1966); (ii) the velocity coplanarity method, VC (Abraham-Shrauner, 1972); and (iii) the three mixed methods, MD1, MD2 and MD3, of Abraham-Shrauner and Yun (1976). The MC and VC methods show limitations due to the adopted assumptions, and the MD methods fail when the shock is perpendicular and they give poor results for quasi-perpendicular shocks (see more details, for example, in Koval and Szabo, 2008). The most robust method is the MD3, where $\hat{n}$ is derived from

$$\hat{n} = \pm \frac{((\vec{B}_d - \vec{B}_u) \times (\vec{v}_d - \vec{v}_u)) \times (\vec{B}_u - \vec{B}_d)}{|((\vec{B}_d - \vec{B}_u) \times (\vec{v}_d - \vec{v}_u)) \times (\vec{B}_u - \vec{B}_d)|}, \qquad (2)$$

where the subscripts u and d refer to upstream and downstream values, respectively. Note that we calculate the normal direction to the shock front directed Sunward, hence, in the opposite sense of the plasma flow.

The method developed by Viñas and Scudder (1986) and Szabo (1994) is the most comprehensive method for shock parameter determination from single spacecraft magnetic field and plasma observations (Koval and Szabo, 2008). But this technique is currently only applicable to single-point shock measurements as visual inspection is needed; thus, it is not adapted yet for automatic application to hundreds of points (cobpoints) at the front of a simulated shock. Therefore, here we applied the five aforementioned methods to determine the shock normal at the cobpoint, mainly relaying on the outputs given by the MD3 method.

As an example of the performed procedure, Fig. 3 shows the calculated IMF line (red trace), the location of the cobpoint (black solid circle) and the shock normal directions obtained by using the five methods previously described (color coded as described in the top central insert of the two large images), for the N22W00 observer (brown solid circle) and for a snapshot of the simulation at $t = 4.95$ h. Top large image is a 2D view of the XY plane and the color scale represents v_r-contours for the slice corresponding to the Z-coordinate of the cobpoint. Bottom large image is a view of the XZ plane with the v_r-contours for the slice corresponding to the Y-coordinate of the cobpoint (this figure is mirrored with respect to the top image in order to better show the computed normals and the observer–Sun line). The two small figures are zoomed out views of the respective figures to quantify the radial distances involved. The maximum angle between two of these five normals is smaller than 2°, and smaller than 0.1° within the normals calculated using the MD methods. This behavior holds for the other eight observers, being the maximum angular difference between two of these normals smaller than 1.2° at a given cobpoint for the N22W45 observer.

Once the shock normal direction is determined, we look for the definitive "downstream point" searching along the normal line, from the cobpoint toward the Sun. This downstream point is the first point after the cobpoint where velocity and density start decreasing.

The final step of this procedure is to calculate the upstream-to-downstream ratio across the shock front, for any plasma variable of the simulation we are interested to study (the velocity, density and magnetic field ratios or the θ_{Bn} angle, for example). Note that, as these quantities are calculated in the normal direction at the cobpoint, we are implicitly assuming that the spatial structure of the shock does not change significantly for short periods of time (as accepted for observations with only one spacecraft). In the next section we present part of the results obtained, mainly focusing in the normalized radial velocity jump, $\mathrm{VR} = \frac{v_r(d)}{v_r(u)} - 1$, being $v_r(u)$ and $v_r(d)$ the radial velocity at the upstream and downstream point, respectively. This is the variable used in our 2D or 2.5D MHD shock-and-particle model to quantify the strength of the shock at the cobpoint (see, for example, Heras et al., 1995; Lario et al., 1998; Aran et al., 2007, for more details). These calculations have been performed on the SGI Altix 3700 machine of the CESCA (Centre de Supercomputació de Catalunya) supercomputing center.

4. Results and discussion

4.1. Solar wind plasma and interplanetary magnetic field evolution

Fig. 4 shows from top to bottom the evolution of B, n and v_r of the solar wind as measured for each one of the

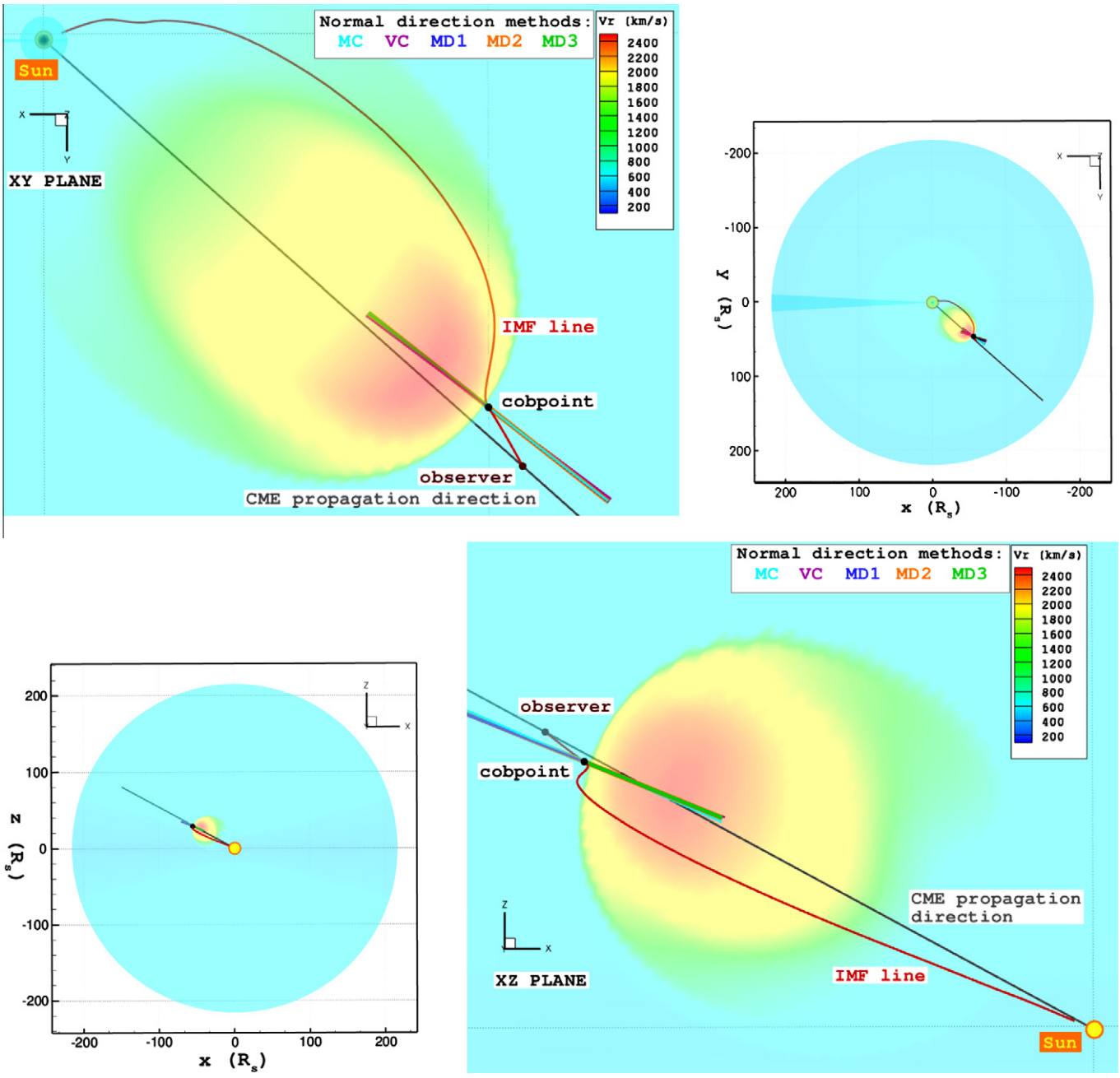

Fig. 3. Two views of the same snapshot as the previous figure. Top: a general (right) and a zoomed (left) view of the *XY* plane; bottom: the same for the *XZ* plane. Contours of plasma radial velocity are color coded as indicated in the top right bars. The Sun is the yellow point. The brown point marks the position of the N22W00 observer and the red line its IMF line. The cobpoint is drawn in black. The black line indicates the CME propagation direction. The rest of the colored lines show the different normal directions obtained from applying the methods described in the text; the top horizontal insert identifies each method with a color.

nine observers described in Section 3. The shock passage occurs between 5 and 13 h after the launch of the CME, depending on the position of each observer (despite that all of them are located at 86 $R_\odot$). Left, middle and right vertical panels correspond, respectively, to observers located at W45, W00 and E30 longitude. In each panel, the solid, dotted and dashed lines correspond to the N37, N22 and N07 observers' latitude, respectively, as labeled.

As can be seen, the background or upstream plasma and IMF conditions differ due to the change of the magnetic field and solar wind density and velocity with latitude (see also Fig. 1). As a consequence of the changes in the solar wind velocity, the longitude of the cobpoint also changes with the latitudinal position of the observer. Table 1 displays the location at the shock front where the first magnetic connection between the observer and the

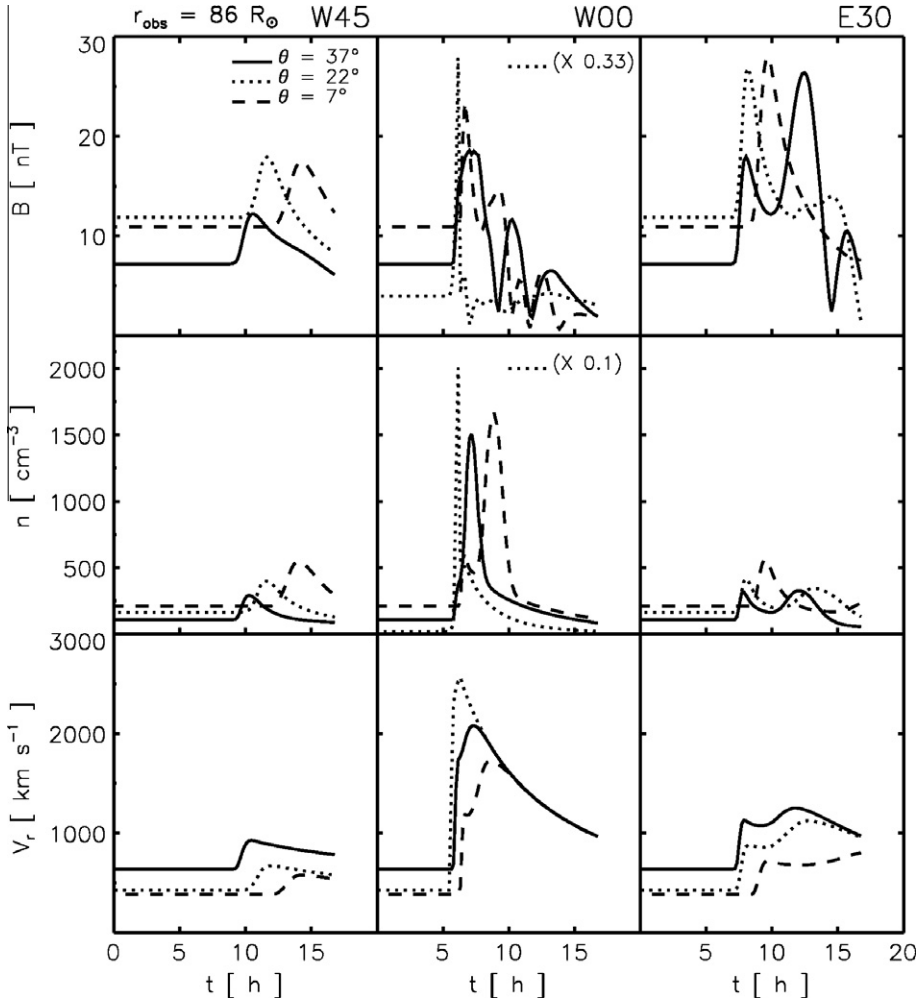

Fig. 4. From top to bottom: evolution of B, n and v_r as seen by the nine observers described in the text. Each column shows the longitude of the observer and each style of line represents its latitude, as labeled. The dotted curves of the two top panels in the middle column had been reduced by the factor specified in the plot.

Table 1
Location of the first magnetic connection of each observer with the shock front.

$\theta = 7°$			$\theta = 22°$			$\theta = 37°$		
W45	W00	E30	W45	W00	E30	W45	W00	E30
N07W23	N07E23	N07E53	N22W23	N22E22	N22E52	N37W30	N37E16	N37E46

shock is established (i.e., the first cobpoint for each observer), as derived from the MHD model. Differences in the cobpoint longitude in the first connection between N07 and N37 observers, with the same longitude, are of about 7°.

In addition to these variations, due to the solar wind velocity variation in latitude, the shock itself travels at different velocities depending on the latitude (and longitude). This makes the relative cobpoint positions of the different observers change with time as the shock expands into the interplanetary medium. Furthermore, the cobpoint location also depends on the direction in which the shock propagates and on the curvature of the front in latitude (and longitude). In the same way as wide and narrow CMEs exist (and their driven shocks), it could happen that a shock is narrower in latitude than in longitude with respect to its nose (or vice versa); nature does not distinguish between them. We obtain the position of the cobpoint from the MHD model following the procedure described in the previous section.

The shock arrives first to the central meridian observers (middle column of Fig. 4) for which their cobpoints scan the central regions of the shock front: (i) from approximately 23° to the left up to the nose of the shock, for the case of the N07W00 observer, and (ii) from ~22° and ~16° for the other two central meridian observers,

N22W00 and N37W00, respectively (see Table 1). The shortest transit time of the shock from the Sun corresponds to the observer located in the same direction as the nose of the shock, N22W00; this is a straightforward result from the fact that this is the CME-launch direction (where the maximum initial momentum is directed to), being the central region of the shock front the fastest region. Only 10 min later the shock arrives to the observer with the highest latitude, N37W00, and 41 min later to the observer at N07W00. The reason of this difference is that the background solar wind speeds for these observers are quite different: 626, 422 and 380 km s^{-1} for the N37, N22 and N07 observers, respectively. In the case of the western (eastern) observers their cobpoint scans the right (left) wing of the shock as it expands into the interplanetary space. For these observers (see left and right columns of Fig. 4), the higher is their latitude the earlier the shock reaches them because of the higher background speed of the solar wind. Moreover, the difference on the arrival times among observers placed at the same heliocentric longitude increases with increasing longitude separation from the nose of the shock.

The increase observed in magnetic field intensity, solar wind density and velocity at the shock front passage (i.e., the jump in the plasma variables) by each spacecraft is larger for the central meridian observers at all latitudes. This just means that the shock strength is higher for longitudes close to the nose of the shock, as already reported in different studies (e.g., Smith and Dryer, 1990; Heras et al., 1995; Aran et al., 2005). If we compare the three central meridian events (middle column of Fig. 4), the downstream-to-upstream magnetic field ratios derived for the N37W00 and N07W00 observers are ~2.5 and ~2.1, respectively. These values are within the range of values reported from Helios observations at 0.4 AU (Volkmer and Neugebauer, 1985). The observer placed at the nose of the shock (at the time of the shock arrival), N22W00, shows the maximum magnetic field compression, with a downstream value of ~81 nT, which is also a reasonable value. For instance, the Helios-1 spacecraft was located at 0.36 AU during the shock passage of the event on May 7 1978 and at 0.40 AU at the passage of the shock associated with the SEP event on June 8 1980. The downstream magnetic field values recorded in these events are about 72 and 67 nT, respectively. In the SEP event on April 28 1978, Helios-1 (at 0.31 AU) measured ~108 nT just after the shock crossing. Note that the upstream magnetic field for these events varied between 30 and 40 nT and hence the background field of the model (that varies in latitude from 8 to 12 nT) underestimates by a factor of approximately three the actual background IMF intensity. This leads to obtain a magnetic field ratio across the shock of ~6.7 instead of ~2.3, if the background field intensity value were closer to that observed.

The central panel of Fig. 4 shows the particle density recorded at the three central meridian observers. The upstream solar wind number density varies from 100 cm^{-3} for the highest latitude to ~220 cm^{-3} near the ecliptic plane. At 1 AU, near the ecliptic plane ($\theta = 7°$), the model gives a density of $n \sim 37\ cm^{-3}$, a factor ~7 higher than the usually observed value (5 cm^{-3}). This, together with the fact that we have introduced a high-density and high-velocity initial blob, explains these too high densities at the shock passage for the central meridian observers. Furthermore, a contribution to this density (and magnetic field) increase just behind the shock may also come from the existence of an indentation in the shock front, formed as a consequence of the bimodal structure of the background solar wind, as described by Manchester et al. (2005).

The bottom panel of the middle column of Fig. 4 shows the evolution of the solar wind radial velocity for these same observers. The values measured at the shock arrival are good taking into account that the CME is very fast, and consequently, it pushes ahead a very fast interplanetary forward shock. For example, in the case of the SEP event on October 28, 2003, the solar wind speed reached values close to 2000 km s^{-1} just after the shock passage (Lario et al., 2008). The normalized radial velocity jump across the shock, VR, for the N22W00 observer is 3.8, and for the northern and southern observers are 1.8 and 2.3, respectively. Note that the solar wind velocity matches the velocity values observed either at 1 AU and at 0.4 AU. There are not significant differences when comparing the jumps obtained at different latitudes for the W45 observers (left column in Fig. 4) and for the E30 observers (right column in Fig. 4).

4.2. Evolution of VR and SEP flux profiles

Lario et al. (1998) determined an empirical relation between the injection rate of shock-accelerated protons at the cobpoint position, Q, and the radial velocity jump across the shock, VR : $\log Q \propto$ VR. This Q(VR) relation has allowed us to generate proton intensity profiles as seen at different locations in the heliosphere (e.g., Lario et al., 1998; Aran et al., 2007) and to generate the tool SOLPENCO (Aran et al., 2006, 2008), a first step towards the prediction of SEP event intensities and fluences in space weather. Fig. 5 illustrates the evolution of VR for the nine observers. As in Fig. 4, the three panels show, from left to right, the evolution of VR for the W45, W00 and E30 observers, respectively. The solid, dotted and dashed lines correspond to the N37, N22 and N07 locations.

For the central meridian observers the first connection with the shock front occurs very early in the event, i.e., in the first 30 min after the launch of the CME. It is established when the shock is close to the Sun, from 4.8 $R_\odot$ for the N37 observer to 6.0 $R_\odot$ for the N07 observer (note that this is much closer to the Sun than 18 $R_\odot$), and also close to the shock nose in longitude (<23°, see Table 1). At this time the values of VR for the three observers are very high, from 7.1 to 8.2. Then, VR decreases rapidly in the first 2–3 h, within $r \sim 34\ R_\odot$ to $r \sim 40\ R_\odot$ from the Sun. This implies that the injection rate on shock-accelerated particles at the

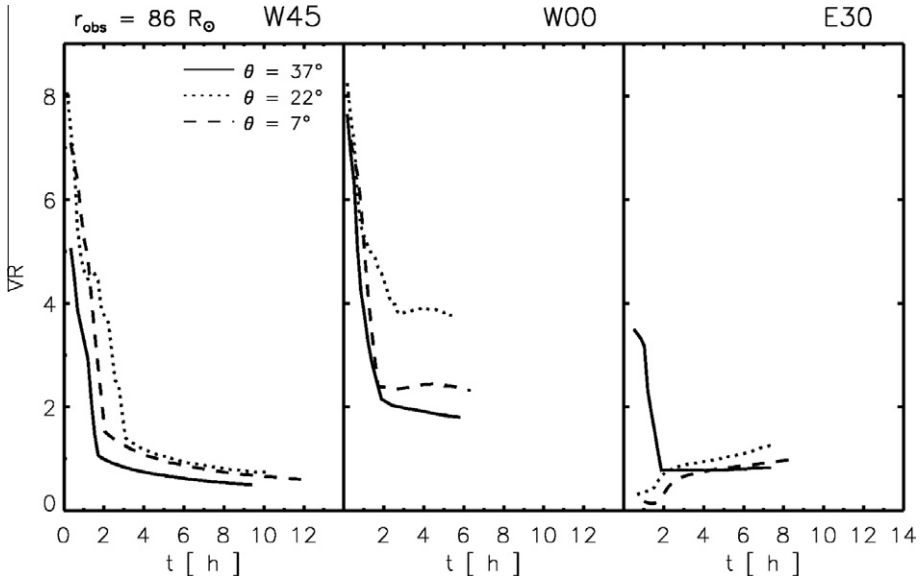

Fig. 5. Evolution of VR at the cobpoint for the nine observers described in the text. Each column shows the longitude of the observer and each type of line represents its latitude, as labeled.

early phase of the event will be the highest throughout the event and it will take place near the Sun, as expected for a good connection between the observer and the shock front. Moreover, depending on the latitude the values of VR can be quite different, and thus those of the injection rate (as we quantify below).

For the western events (left panel of Fig. 5), VR resembles that of the central meridian events. The first magnetic connection for the N07 and N22 observers is established at N07W23 and N22W23, respectively, and the initial values of VR are similar to the ones of the corresponding central meridian event. The lower value of VR attained for the northern observer comes from the fact that its first magnetic connection is established at N37W30. Since the cobpoint of the western observers scans the right wing of the shock front as the shock reaches them, VR decreases to lower values than for the central meridian observers. Such values are ordered in latitudinal distance from the nose of the shock, that is the closer the observer in latitude with respect to the nose of the shock the higher the obtained value of VR. In order to understand this, note that if we measure the coordinates of the observers with respect to a XY plane tilted 22° northward the equatorial plane, i.e., containing the direction of the nose of the shock, the positions of the N37W45, N22W45 and N07W45 observers are N20W37, N06W41 and S09W45, respectively.

For the N07 and N022 eastern events (dashed and dotted lines, respectively, in the right panel in Fig. 5) VR follows a different evolution from the western and central meridian events. For these observers, VR increases with time because their magnetic connection is established, in longitude, far from the nose of the shock along the left wing, starting from E53 and E52 locations. As for the western events, the values of VR are organized with increasing separation in latitude from the nose of the shock. The northern observer, instead, is connected closer to the central part of the shock from the beginning, at N20E38. Therefore, the observer is connected to a central region of the shock front and of the downstream region, as suggested by the downstream magnetic field evolution for this observer (top right panel of Fig. 4) which is similar to those of the central meridian events.

To visualize and quantify the influence of the latitude factor on SEP events, through the evolution of VR already commented, we use the particle transport model developed by Lario et al. (1998) to produce synthetic SEP flux profiles, as measured by the nine observers formerly described. The details of the model can be found elsewhere (e.g., Lario et al., 1998; Aran et al., 2007) and the values adopted for the description of the interplanetary particle transport and other features of the model can be found in Aran et al. (2006). The relevant point, at what makes the difference in the simulated SEP flux profiles, is the source function term Q of the transport equation (Eq. (1) of Lario et al. (1998)). As we assume a functional dependence $Q = Q(\mathrm{VR})$, the evolution of VR described in Fig. 5, for different observers, directly translates into an evolution of Q and, therefore, in a variety of SEP flux profiles (with no other change of any feature or parameter of the model).

Left panel of Fig. 6 shows two sets of SEP flux profiles for the three central meridian observers at different latitudes (identified as in Fig. 5) located at 86 $R_\odot$, for 1 and 32 MeV proton energies. The onset of the event shows velocity dispersion for the two energies considered, as expected. At a given energy, there are also small time differences in the onset of each profile because, depending on the latitude, the magnetic connection between the shock and the observer occurs at slightly different time and place. Moreover, the shock passage also varies with the latitude (both aspects have been previously commented in this sec-

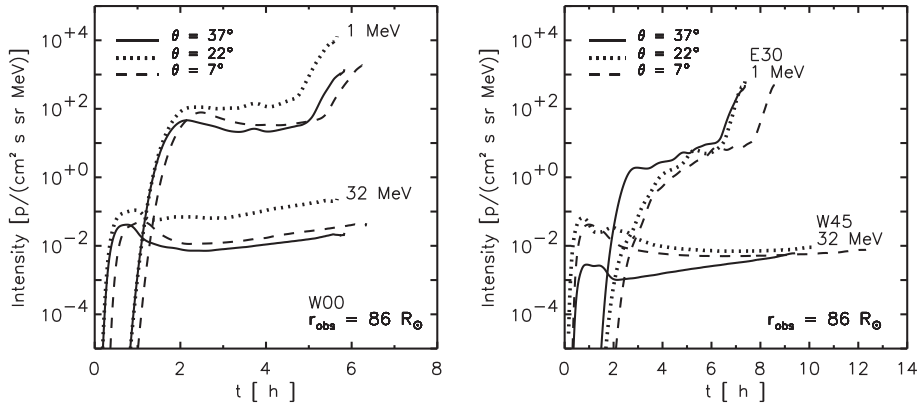

Fig. 6. Simulated SEP time-intensity profiles derived from the Lario et al. (1998) model, after using the VR-values obtained. Left panel: profiles observed for the three W00 observers, located at 86 $R_\odot$ and at different latitudes (see labels and text), for 1-MeV and 32-MeV protons. Right panel: SEP profiles as in the right panel, but for the three E30 observers at different latitudes, for 1-MeV protons, and for three W45 observers, for 32-MeV protons.

tion). As $\log Q \propto$ VR, small differences in VR can yield important flux variations. For example, the value of VR for the N22W00 and N07W00 observers after 3 h is roughly constant (~4 for the first and ~2.4 for the second; see Fig. 5). This difference in the VR values translates, by means of the adopted Q(VR) relation, into an injection rate of about six times higher in the cobpoint of the N22W00 observer than in the case of the N07W00 observer. Hence, their respective flux profiles (dotted and dashed traces in left panel of Fig. 6) show similar differences in their evolution as for Q during this period. As a result of the evolution of VR it derives that the closer the observer's latitude is to the shock nose latitude, the larger is the attained proton flux; it could be a factor 10 during several hours after the prompt phase of the event (e.g., dotted and solid traces).

Right panel of Fig. 6 shows two other sets of synthetic SEP intensity–time profiles for observers located at the same latitudes shown in the left panel. The first set consists of 1-MeV proton fluxes as seen by the three observers located at E30 and the second set shows 32-MeV proton fluxes for the three observers located at W45. Both sets measure proton fluxes less intense than the corresponding fluxes for the observers placed at central meridian locations, mainly as a consequence of the different regions of the front shock scanned by their cobpoints and hence, the different evolution of VR. Again, note that the change in latitude in the position of a western observer could lead to a difference in the peak intensity ratio (attained at the prompt phase of the event) of one order of magnitude.

5. Conclusions

We have developed a procedure to automatically determine the location of the cobpoint, the corresponding shock normal and the downstream point for three-dimensional simulations. We have applied this procedure to nine observers located at ~0.4 AU, at vantage points with different heliocentric longitudes and latitudes by using a 3D MHD model to simulate the propagation of a CME-driven shock up to 100 $R_\odot$.

We have analyzed the evolution of the magnetic field intensity, number density and radial velocity for these observers discussing the relevance of the latitude of the observer, a factor scarcely commented and quantitatively not addressed in numerical simulations of SEP events. At present, practically all efforts in that sense have been focused in the longitude (or heliolongitude) component, mainly because: (i) the main body of observations comes from spacecraft located near 1 AU and near to the ecliptic plane; and (ii) 3D modeling of SEP events is a complex and computer demanding task hardly affordable, even nowadays.

We have studied the evolution of the normalized radial velocity jump, VR, for these nine observers, showing that: (i) MHD simulations of shocks have to include the evolution of the plasma variables and magnetic field close to the Sun (i.e., below 18 $R_\odot$), since the strength of the shock, represented here by VR, rapidly decreases with radial distance, and hence, the efficiency of the shock as particle accelerator (especially important at high energies); and (ii) the VR also depends on the latitude, not only on the longitude. Therefore, 3D models should take into account the influence of the variations of the plasma variables at the shock front with latitude.

We have presented examples of the importance of the latitude of the observer with respect to the approaching CME-driven shock, by synthesizing several SEP flux profiles, within the frame of our shock-and-particle model. Peak intensities (and also fluences) could largely change - up to one order of magnitude – for observers at vantage points with the same longitude but different latitudes. In short, the latitude factor is relevant for space weather forecasting purposes and, therefore, it deserves further attention.

Acknowledgments

The authors are grateful to S.T. Wu, A.H. Wang, A. Viñas for productive discussions on the subject. This research work

is supported by the Ministerio de Ciencia e Innovación (Spain) under the project AYA2007-60724. A.A. is supported by an ESA internal research fellowship. C.J. acknowledges support from Grant 3E090665 (FWO-Vlaanderen). Financial support from the projects GOA/2009-009 (K.U. Leuven), G.0304.07 (FWO-Vlaanderen), C 90347 (ESA Prodex 9), SOLAIRE Network (MTRN-CT-2006-035484), and the SOTERIA project (FP7/2007-2013 Grant Agreement No. 218816) is gratefully acknowledged. The authors acknowledge the use of the computing facilities of the supercomputer cluster of CESCA (Centre de Supercomputació de Catalunya), the supercomputer MareNostrum, from the BSC (Barcelona Supercomputing Center) and the high performance cluster VIC at the KUL (Katholieke Universiteit Leuven). R.R.-G. wants to render thanks to L. Bettarini for useful discussions and suggestions.

References

Abraham-Shrauner, B. Determination of magnetohydrodynamic shock normals. J. Geophys. Res. 77, 736–739, 1972.

Abraham-Shrauner, B., Yun, S.H. Interplanetary shocks seen by AMES plasma probe on Pioneer 6 and 7. J. Geophys. Res. 81, 2097–2102, 1976.

Aran, A., Lario, D., Sanahuja, B., Marsden, R.G., Dryer, M., Fry, C.D., McKenna-Lawlor, S.M.P. Modeling and forecasting solar energetic particle events at Mars: the event on 6 March 1989. A&A 469, 1123–1134, 2007.

Aran, A., Sanahuja, B., Lario, D. Fluxes and fluences of SEP events derived from SOLPENCO. Ann. Geophys. 23, 3047–3053, 2005.

Aran, A., Sanahuja, B., Lario, D. SOLPENCO: a solar particle engineering code. Adv. Space Res. 37, 1240–1246, 2006.

Aran, A., Sanahuja, B., Lario, D. Comparing proton fluxes of central meridian SEP events with those predicted by SOLPENCO. Adv. Space Res. 42, 1492–1499, 2008.

Berdichevsky, D.B., Szabo, A., Lepping, R.P., Viñas, A.F., Mariani, F. Interplanetary fast shocks and associated drivers observed through the 23rd solar minimum by Wind over its first 2.5 years. J. Geophys. Res. 105, 27289–27314, 2000.

Cane, H.V., Lario, D. An Introduction to CMEs and Energetic Particles. Space Sci. Rev. 123, 45–56, 2006.

Cane, H.V., Reames, D.V., von Rosenvinge, T.T. The role of interplanetary shocks in the longitude distribution of solar energetic particles. J. Geophys. Res. 93, 9555–9567, 1988.

Colaninno, R.C., Vourlidas, A. First determination of the true mass of coronal mass ejections: a novel approach to using the two STEREO viewpoints. ApJ 698, 852–858, 2009.

Colburn, D.S., Sonett, C.P. Discontinuities in the Solar Wind. Space Sci. Rev. 5, 439–506, 1966.

Domingo, V., Sanahuja, B., Heras, A.M. Energetic particles, interplanetary shocks and solar activity. Adv. Space Res. 9, 191–195, 1989.

Evans, C.R., Hawley, J.F. Simulation of magnetohydrodynamic flows – a constrained transport method. ApJ 332, 659–677, 1988.

Evenson, P., Meyer, P., Yanagita, S. Solar flare shocks in interplanetary space and solar flare particle events. J. Geophys. Res. 87, 625–631, 1982.

Groth, C.P.T., de Zeeuw, D.L., Gombosi, T.I., Powell, K.G. Three-dimensional MHD simulation of coronal mass ejections. Adv. Space Res. 26, 793–800, 2000.

Hapgood, M.A. Space physics coordinate transformations – a user guide. Planet. Space Sci. 40, 711–717, 1992.

Heras, A.M., Sanahuja, B., Lario, D., Smith, Z.K., Detman, T., Dryer, M. Three low-energy particle events: modeling the influence of the parent interplanetary shock. ApJ 445, 497–508, 1995.

Heras, A.M., Sanahuja, B., Smith, Z.K., Detman, T., Dryer, M. The influence of the large-scale interplanetary shock structure on a low-energy particle event. ApJ 391, 359–369, 1992.

Jacobs, C., Magnetohydrodynamic Modelling of the Solar Wind and Coronal Mass Ejections. Ph.D. thesis, Katholieke Universiteit Leuven, Leuven, Belgium, 2007.

Jacobs, C., Poedts, S., Van der Holst, B., Chané, E. On the effect of the background wind on the evolution of interplanetary shock waves. A&A 430, 1099–1107, 2005.

Jacobs, C., van der Holst, B., Poedts, S. Comparison between 2.5D and 3D simulations of coronal mass ejections. A&A 470, 359–365, 2007.

Kahler, S.W. The correlation between solar energetic particle peak intensities and speeds of coronal mass ejections: effects of ambient particle intensities and energy spectra. J. Geophys. Res. 106, 20947–20956, 2001.

Koval, A., Szabo, A. Modified "Rankine-Hugoniot" shock fitting technique: simultaneous solution for shock normal and speed. J. Geophys. Res. 113 (A12), A10110-1–A10110-9, 2008.

Lario, D., Aran, A., Decker, R.B. Major solar energetic particle events of solar cycles 22 and 23: intensities above the streaming limit. Space Weather 6, S12001-1–S12001-25, 2008.

Lario, D., Sanahuja, B., Heras, A.M. Energetic particle events: efficiency of interplanetary shocks as 50 kev $<$ e $<$ 100 mev proton accelerators. ApJ 509, 415–434, 1998.

Li, G., Zank, G.P., Desai, M.I., Mason, G.M., Rice, W.K.M. Particle acceleration and transport at CME-driven shocks: a case study, in: Gallagher, D.L., Horwitz, J.L., Perez, J.D., Preece, R.D., Quenby, J.J. (Eds.), Particle Acceleration in Astrophysical Plasmas: Geospace and Beyond. Geophysical Monograph 156, AGU, Washington, pp. 51–58, 2005.

Lin, C.C., Chao, J.K., Lee, L.C., Lyu, L.H., Wu, D.J. A new shock fitting procedure for the MHD Rankine–Hugoniot relations for the case of small He^{2+} slippage. J. Geophys. Res. 111 (A10), A9104-1–A9104-26, 2006.

Lugaz, N., Manchester IV, W.B., Gombosi, T.I. Numerical simulation of the interaction of two coronal mass ejections from sun to earth. ApJ 634, 651–662, 2005a.

Lugaz, N., Manchester IV, W.B., Gombosi, T.I. The evolution of coronal mass ejection density structures. ApJ 627, 1019–1030, 2005b.

Luhmann, J.G., Ledvina, S.A., Krauss-Varban, D., Odstrcil, D., Riley, P. A heliospheric simulation-based approach to SEP source and transport modeling. Adv. Space Res. 40, 295–303, 2007.

Manchester, W.B., Gombosi, T.I., De Zeeuw, D.L., Sokolov, I.V., Roussev, I.I., Powell, K.G., Kóta, J., Tóth, G., Zurbuchen, T.H. Coronal mass ejection shock and sheath structures relevant to particle acceleration. ApJ 622, 1225–1239, 2005.

Manchester, W.B., Gombosi, T.I., Roussev, I., De Zeeuw, D.L., Sokolov, I.V., Powell, K.G., Tóth, G., Opher, M. Three-dimensional MHD simulation of a flux rope driven CME. J. Geophys. Res. 109 (A18), A1102-1–A1102-17, 2004a.

Manchester, W.B., Gombosi, T.I., Roussev, I., Ridley, A., De Zeeuw, D.L., Sokolov, I.V., Powell, K.G., Tóth, G. Modeling a space weather event from the Sun to the Earth: CME generation and interplanetary propagation. J. Geophys. Res. 109 (A18), A2107-1–A2107-15, 2004b.

Manchester, W.B., Ridley, A.J., Gombosi, T.I., Dezeeuw, D.L. Modeling the Sun-to-Earth propagation of a very fast CME. Adv. Space Res. 38, 253–262, 2006.

Manchester IV, W.B., Vourlidas, A., Tóth, G., Lugaz, N., Roussev, I.I., Sokolov, I.V., Gombosi, T.I., De Zeeuw, D.L., Opher, M. Three-dimensional MHD simulation of the 2003 October 28 coronal mass ejection: comparison with LASCO coronagraph observations. ApJ 684, 1448–1460, 2008.

Parker, E.N. Dynamics of the interplanetary gas and magnetic fields. ApJ 128, 664–676, 1958.

Reames, D.V. Acceleration of energetic particles by shock waves from large solar flares. ApJ Lett. 358, L63–L67, 1990.

Richardson, I.G., Cane, H.V., von Rosenvinge, T.T. Prompt arrival of solar energetic particles from far eastern events – the role of large-scale

interplanetary magnetic field structure. J. Geophys. Res. 96, 7853–7860, 1991.

Smith, Z., Dryer, M. MHD study of temporal and spatial evolution of simulated interplanetary shocks in the ecliptic plane within 1 AU. Sol. Phys. 129, 387–405, 1990.

Sokolov, I.V., Roussev, I.I., Gombosi, T.I., Lee, M.A., Kóta, J., Forbes, T.G., Manchester, W.B., Sakai, J.I. A new field line advection model for solar particle acceleration. ApJ Lett. 616, L171–L174, 2004.

Szabo, A. An improved solution to the 'Rankine–Hugoniot' problem. J. Geophys. Res. 99, 14737–14746, 1994.

Tóth, G. A general code for modeling MHD flows on parallel computers: versatile advection code. Astrophys. Lett. Commun. 34, 245–251, 1996.

Verkhoglyadova, O.P., Li, G., Zank, G.P., Hu, Q., Mewaldt, R.A. Using the path code for modeling gradual sep events in the inner heliosphere. ApJ 693, 894–900, 2009.

Viñas, A.F., Scudder, J.D. Fast and optimal solution to the 'Rankine–Hugoniot problem'. J. Geophys. Res. 91, 39–58, 1986.

Volkmer, P.M., Neugebauer, F.M. Statistical properties of fast magnetoacoustic shock waves in the solar wind between 0.3 AU and 1 AU – Helios-1, 2 observations 3, pp. 1–12, 1985.

Vourlidas, A., Buzasi, D., Howard, R.A., Esfandiari, E. Mass and energy properties of LASCO CMEs, in: Kuijpers, J. (Ed.), Solar Variability: From Core to Outer Frontiers, vol. 506 of ESA Special Publication, pp. 91–94, 2002.